

# Open Research Online

---

The Open University's repository of research publications and other research outputs

## Effects of an ionic liquid and processing conditions on the $\beta$ -polymorph crystal formation in poly(vinylidene fluoride)

### Journal Item

#### How to cite:

Pickford, Tom; Gu, Xu; Heeley, Ellen and Wan, Chaoying (2019). Effects of an ionic liquid and processing conditions on the  $\beta$ -polymorph crystal formation in poly(vinylidene fluoride). *CrystEngComm*, 21(36) pp. 5418–5428.

For guidance on citations see [FAQs](#).

© 2019 The Royal Society of Chemistry



<https://creativecommons.org/licenses/by-nc-nd/4.0/>

Version: Supplementary Material

Link(s) to article on publisher's website:  
<http://dx.doi.org/doi:10.1039/C9CE01051C>

---

Copyright and Moral Rights for the articles on this site are retained by the individual authors and/or other copyright owners. For more information on Open Research Online's data [policy](#) on reuse of materials please consult the policies page.

---

## Effects of an ionic liquid and processing conditions on the $\beta$ -polymorph crystal formation in poly(vinylidene fluoride)

Tom Pickford<sup>1</sup>, Xu Gu<sup>1</sup>, Ellen L. Heeley<sup>2\*</sup>, Chaoying Wan<sup>1\*</sup>

<sup>1</sup>International Institute for Nanocomposites Manufacturing (IINM), WMG, University of Warwick, CV4 7AL, UK

<sup>2</sup>Faculty of Science, Technology, Engineering and Mathematics, Open University, Walton Hall, Milton Keynes, MK7 6AA.

Corresponding Authors \*: chaoying.wan@warwick.ac.uk; Ellen.Heeley@open.ac.uk

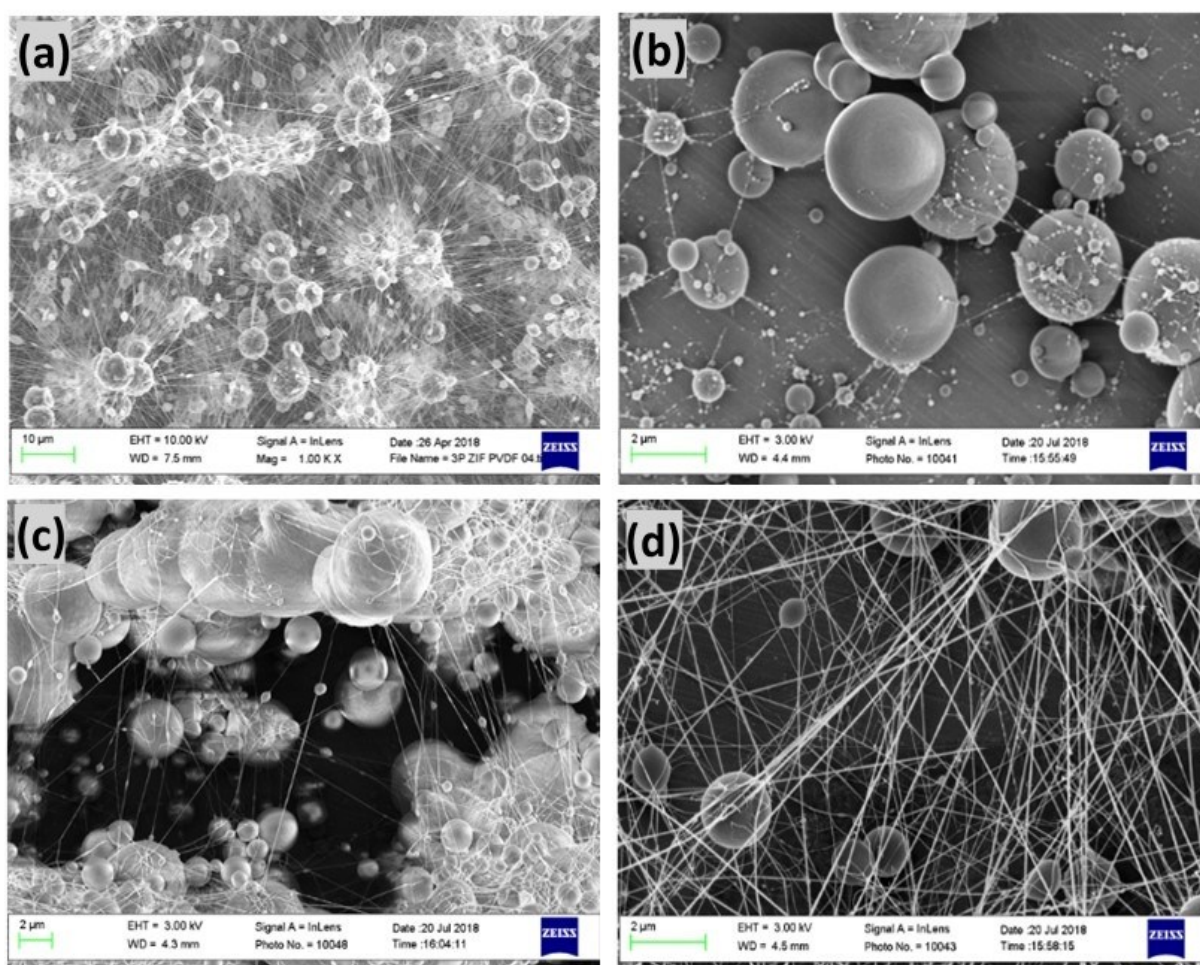


**Figure S1.** SEM images of PVDF nanofibers: **(a)** PVDF 20 wt% in 7:3 DMF/acetone **(b-d)** PVDF in DMF with different concentrations of **(b)** 10 wt%; **(c)** 15 wt% and **(d)** 20 wt%. The fibres shown in **(d)** were formed at a flow rate of 3 ml hr<sup>-1</sup>, a voltage of 12.7 kV and a tip-collector distance of 15 cm

The processing conditions for the electrospinning of our PVDF nanofibres first had to be determined. These are shown in **Figure S1**. The concentration of PVDF in the spinning solution determines the viscosity and surface tension of the spinning solution, which has a significant influence on the

morphology of electrospun fibres. When first attempting electrospinning, PVDF was mixed into DMF/Acetone (7:3 ratio) at 20 wt%, as shown in **Figure S1(a)**. This produced a highly beaded nanofibre membrane via rather unstable electrospinning, suggesting the solution was too volatile. Thus we tried electrospinning with DMF alone, attempting several PVDF concentrations to find an optimal solution viscosity with this change of solvent. When the concentration of PVDF/DMF solution was reduced to 10 wt% or 15 wt% (**Figure S1(b) and S1(c)** respectively), beads were generated to an even greater extent. These low viscosity solutions have low surface tension, which results in the spinning solution being directly sprayed onto the collector under the electric field without jet elongation, producing a film of polymer beads rather than a nanofibre membrane. By increasing the concentration to 20 wt%, a more stable jet was formed resulting in a uniform fibre morphology, although even these fibres are not seen to be completely beadless despite the seemingly stable electrospinning (**Figure S1(d)**). Finally, the relationship between flow rate and electric field strength (the ratio of voltage to tip-collector distance) determines the balance between the electric force on the polymer solution and the surface tension on the droplet of solution formed at the spinneret end. For our nanofibres, this balance was at ~12.7 kV voltage, 3cm tip-collector distance and a flow rate of 3 ml hr<sup>-1</sup>. Typical fibre diameters lie in the range of 50-150 nm for the fibres in **Figure S1(d)**.

**Table S1.** Crystallographic planes identified for each phase from the 1D-WAXS data, for the  $\alpha$ ,  $\beta$  and  $\gamma$  phases of PVDF. Planes denoted in bold are observed as strong peaks in the WAXS data, whereas others are smaller, less distinct peaks. The (132) and (211)  $\gamma$ -phase signatures are difficult to separate, and so are grouped.

Crystal phase	$\alpha$	$\beta$	$\gamma$
Neat PVDF electrospun	<b>(110), (021), (120), (200)</b>	(110), <b>(310)</b> , (020), (101)	<b>(110), (022), (200)</b> , (132)/(211)
PVDF/AMIM electrospun	(110), <b>(140), (200)</b>	<b>(110), (001), (310), (020), (101)</b>	<b>(110)</b> , (200), (132)/(211)
Neat PVDF solution-cast	(110), (002)	<b>(110), (310)</b>	<b>(110), (004), (132)/(211)</b>
PVDF/AMIM solution-cast	(110), (002)	<b>(110), (310)</b>	<b>(110), (004), (132)/(211)</b>
Neat PVDF melt-compressed	<b>(110), (021), (120), (200), (040), (002)</b>	(110)	<b>(110), (022), (200)</b> , (041), (132)/(211)
PVDF/AMIM melt-compressed	(110)	<b>(110)</b> , (020)	<b>(110)</b> , (004)

Table S1 details the full  $hkl$  peaks observed for all samples indicating the major crystal phase present in each case. From this data the  $\alpha$ -phase dominates in the electrospun and melt-compressed neat PVDF samples, whereas the  $\beta$ -phase is quite dominant in the electrospun PVDF/AMIN sample. The solution-cast neat PVDF and PVDF/AMIN show that the  $\beta$ - and  $\gamma$ -phase is prevalent in these samples.